JCTC Journal of Chemical Theory and Computation

Article

pubs.acs.org/JCTC

Attosecond X-ray Diffraction Triggered by Core or Valence Ionization of a Dipeptide

Daeheum Cho,*[,†,‡] Jérémy R. Rouxel,[†] Markus Kowalewski,[†] Jin Yong Lee,*[,§] and Shaul Mukamel*[,†]

[†]Department of Chemistry, University of California, Irvine, California 92697-2025, United States

[‡]School of Advanced Materials Science and Engineering, SKKU Advanced Institute of Nanotechnology (SAINT), Sungkyunkwan University, Suwon 16419, Republic of Korea

[§]Department of Chemistry, Sungkyunkwan University, Suwon 16419, Republic of Korea

Supporting Information

ABSTRACT: With the advancement of intense ultrafast X-ray sources, it is now possible to create a molecular movie by following the electronic dynamics in real time and real space through time-resolved X-ray diffraction. Here we employ real-time time-dependent density functional theory (RT-TDDFT) to simulate the electronic dynamics after an impulse core or valence ionization in the glycine−phenylalanine (GF) dipeptide. The time-evolving dipole moment, the charge density, and the time-resolved X-ray diffraction signals are calculated. The charge oscillation is calculated for 7 fs for valence ionization and 500 as for core ionization. The charge oscillation time scale is comparable to that found in a phenylalanine monomer (4 fs) [*Science* **2014**, *346*, 336] and is slightly longer because of the elongated glycine chain. Following valence ionization, the charge migration across the GF is mediated by the delocalized lone-pair orbitals of oxygen and nitrogen of the electron-rich amide group. The temporal Fourier transform of the dipole moment provides detailed information on the charge migration dynamics and the molecular orbitals involved. Heterodyne-detected attosecond X-ray diffraction signals provide the magnitude and phase of the scattering amplitude in momentum space and can thus be inverted to yield the charge density in real space.

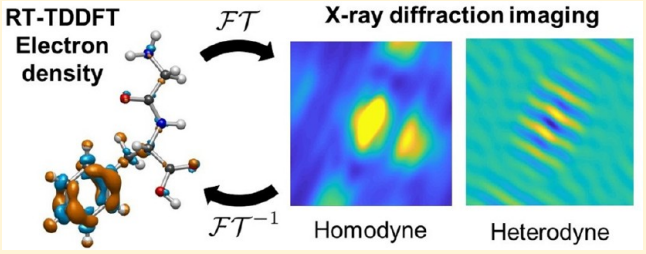

1. INTRODUCTION

Electronic charge density redistribution is the most elementary chemical process. Electron transfer between sites can trigger various photochemical and photophysical processes. Excited-state processes can be investigated by monitoring the electronic response of the system to optical excitation. Real-time and real-space visualization of electronic structure, i.e., creation of molecular movies, is now feasible thanks to new ultrabright and ultrashort X-ray pulses.[1] X-ray diffraction is the standard tool for the determination of the nuclear and electronic structures of solids, liquids, and molecules in the gas phase.[2−5] Time-resolved hard X-ray diffraction[4,6−8] can generate molecular movies because the X-rays have wavelengths comparable to interatomic distances (1 Å for a 12 keV X-ray beam) and attosecond temporal resolution.

Charge transfer across a molecule generally takes hundreds of femtoseconds to picoseconds since it involves nuclear rearrangement. Charge migration, on the other hand, is a purely electronic process induced by electron correlations without the participation of nuclei. Charge migration governs the early electronic dynamics and affects the subsequent charge transfer. It was first reported by Weinkauf et al.,[9] who captured the fragmentation product at a site remote from the initially created hole in isolated peptides. Recently, sub-5 fs charge migration in phenylalanine, an aromatic amino acid, was measured by Nisoli[10] and Greenwood[11] using an extreme-ultraviolet pump and visible/near-infrared probe setup. Extensive Green's function theoretical studies on the mechanism of charge migration and the role of electron correlations were performed by Cederbaum.[12,13] Subfemtosecond charge migration simulations in Tyr-terminated tetrapeptides were reported by Levine.[14] The molecular dynamics of doubly charged uracil in the gas phase has recently been simulated by time-dependent density functional theory (TDDFT).[15] The calculations become rapidly intractable with molecular size because of the prohibitively large number of relevant eigenstates in the ionized states. This is especially true for core ionized states, where many valence states can participate in the dynamics. Recently, Lopata[16] reported a real-time TDDFT (RT-TDDFT) study of the charge migration dynamics following nitrogen K-edge ionization of nitrosobenzene, which demonstrated the robustness of RT-TDDFT to be comparable to that of post-Hartree−Fock methods.

In this work, we used RT-TDDFT to simulate the time-resolved X-ray diffraction signals of the charge migration dynamics following valence or core ionization of the glycine−phenylalanine (GF) dipeptide (see Figure 1). We considered the ionization of either core (amide O 1s and N-terminal N 1s) or valence (N-terminal N lone pair and phenyl chromophore) electrons. The X-ray diffraction signals reveal 7 fs charge migration after valence ionization and 500 as dynamics

Received: September 6, 2017
Published: November 15, 2017

DOI: 10.1021/acs.jctc.7b00920
J. Chem. Theory Comput. 2018, 14, 329−338

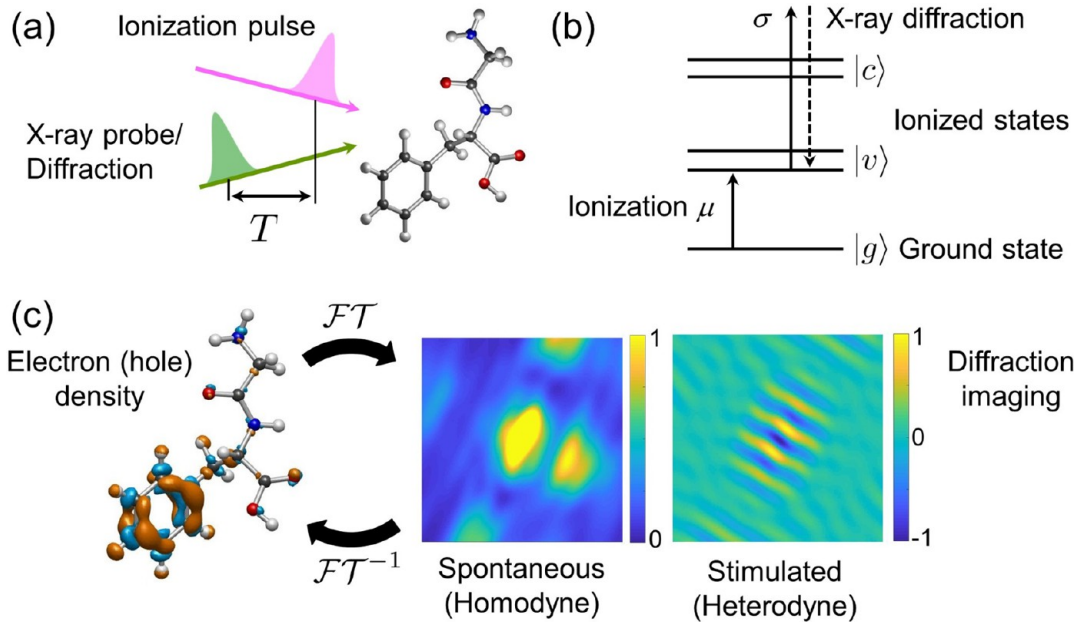

Figure 1. Attosecond X-ray diffraction imaging of electron–hole dynamics following an impulsive ionization. (a) Experimental scheme. The electron–hole dynamics created by an impulsive ionization pump is probed by an X-ray probe pulse after a time delay T. (b) Level scheme (ground state $|g\rangle$, valence ionized states $|v\rangle$, and core ionized states $|c\rangle$) for the X-ray diffraction signals. (c) Inverse Fourier transform ($\mathcal{FT}^{-1}$) of the X-ray diffraction signals recovers the real-space electron–hole density.

following core ionization. Heterodyne detection of the X-ray diffraction signals should allow the signal to be inverted from momentum space to real space. The beating pattern of the dipole moment reveals the electronic states involved.

2. THEORETICAL FRAMEWORK

2.1. Diffraction off the Time-Evolving Charge Density. The electronic charge density is given by the expectation value of the charge density operator $\sigma(\mathbf{r})$:

$$\sigma(\mathbf{r}) = e\psi^{\dagger}(\mathbf{r})\psi(\mathbf{r}) \tag{1}$$

where e is the electron charge and $\psi^{\dagger}(\mathbf{r})$ and $\psi(\mathbf{r})$ are the electron field Fermion creation and annihilation operators at position $\mathbf{r}$, respectively. Diffraction is related to the spatial Fourier transform of the charge density operator:

$$\sigma(\mathbf{q}) = \int \mathrm{d}\mathbf{r}\, \mathrm{e}^{-\mathrm{i}\mathbf{q}\cdot\mathbf{r}}\sigma(\mathbf{r}) \tag{2}$$

where $\mathbf{q} = \mathbf{k}_s - \mathbf{k}_x$ is the scattering vector where $\mathbf{k}_s$ and $\mathbf{k}_x$ are the scattered and incoming X-ray wavevectors, respectively. Diffraction signals are usually measured in the spontaneous (homodyne) detection mode:[17]

$$S_{\mathrm{hom}}(\mathbf{q}) \propto 2\left|\int \mathrm{d}t\, \mathrm{e}^{-\mathrm{i}\omega_s t}\mathbf{A}_X^{*}(t)\langle\sigma(\mathbf{q}, t)\rangle\right|^2 \tag{3}$$

where $\mathbf{A}_X$ is the vector potential envelope of the diffracted X-ray pulse, ω_s is the scattered photon frequency, and $t = 0$ is the ionization time that triggers the electronic dynamics.

Alternatively, the stimulated coherent (heterodyne) diffraction signal[17] created by a single molecule, which employs two pulses with envelopes $\mathbf{A}_X$ and $\mathbf{A}_{\mathrm{het}}$, is given by

$$S_{\mathrm{het}}(\mathbf{q}) \propto 2\Im\int \mathrm{d}t\, \mathbf{A}_{\mathrm{het}}(t)\mathbf{A}_X(t)\langle\sigma(\mathbf{q}, t)\rangle \tag{4}$$

The heterodyne signal requires two coincident, non-collinear X-ray pulses with a controlled relative phase. We shall track the hole dynamics following ionization, focusing on the hole density, which is given by the difference between the time-evolving charge densities in the ionic state and the neutral ground state: $\langle\sigma(\mathbf{q}, t)\rangle_{\mathrm{hole}} = \langle\sigma(\mathbf{q}, t)\rangle_{\mathrm{ion}} - \langle\sigma(\mathbf{q}, t)\rangle_{\mathrm{neutral}}$. S_{het} is useful for monitoring signals from the difference density directly, such as the hole density in the ionized molecule and the electron–hole pair in the excited molecule. The heterodyne signal is linear in the charge density and such differences can easily be carried out, unlike for the homodyne signal expressed as a squared amplitude. The signal from the difference density can be obtained by subtracting the two signals.

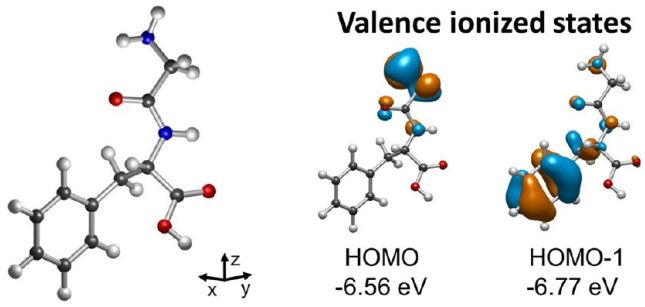

Figure 2. (left) Molecular structure of the glycine–phenylalanine (GF) dipeptide. (right) Valence molecular orbitals HOMO and HOMO−1 (isovalue of 0.04).

$$S_{\mathrm{het}}(\langle\sigma(\mathbf{q}, t)\rangle_{\mathrm{hole}}) = S_{\mathrm{het}}(\langle\sigma(\mathbf{q}, t)\rangle_{\mathrm{ion}}) - S_{\mathrm{het}}(\langle\sigma(\mathbf{q}, t)\rangle_{\mathrm{neutral}}) \tag{5}$$

This is different from the conventional homodyne-detected signal (eq 3), which gives the square of the density and thus measures the square of the difference density.

2.2. RT-TDDFT Calculation of the Signal. Many theoretical approaches have been used to model excited-state dynamics, including time-dependent Hartree–Fock,[18] TDDFT,[19] coupled cluster,[20] and multiconfigurational self-consistent field calculations,[21] in conjunction with nuclear dynamics methods

DOI: 10.1021/acs.jctc.7b00920
J. Chem. Theory Comput. 2018, 14, 329–338

such as Born−Oppenheimer molecular dynamics,[22] Ehrenfest dynamics,[15] and surface hopping.[23,24] A time domain approach that explicitly propagates the electron dynamics in an external field is a natural for describing ultrafast spectroscopy. RT-TDDFT[19,25−28] has been successfully applied to compute absorption spectra of large molecules,[29] core excitation,[30] polaron pair formation,[31] charge transfer,[32,33] light absorption of a photocatalyst,[34] and molecular conductance.[35]

We used RT-TDDFT as implemented in NWChem[36,37] to simulate the charge migration dynamics after core or valence ionization of GF. The dynamics is obtained by solving equations of motion for the reduced single-electron density matrix $\rho(t)$, rather than expanding in eigenstates:[38]

$$i\frac{\partial\rho(t)}{\partial t} = [\mathbf{F}(t), \rho(t)] \tag{6}$$

(in au), where the time-dependent Fock matrix $\mathbf{F}(t)$ is given by[37]

$$\mathbf{F}[\rho(t)] = \mathbf{H}^{\text{core}} + \mathbf{G}^{J}[\rho(t)] + \alpha\mathbf{G}^{K}[\rho(t)] + \beta\mathbf{G}^{\text{X-DFT}}[\rho(t)] + \gamma\mathbf{G}^{\text{C-DFT}}[\rho(t)] - \boldsymbol{\mu}\cdot\mathbf{E}(t) \tag{7}$$

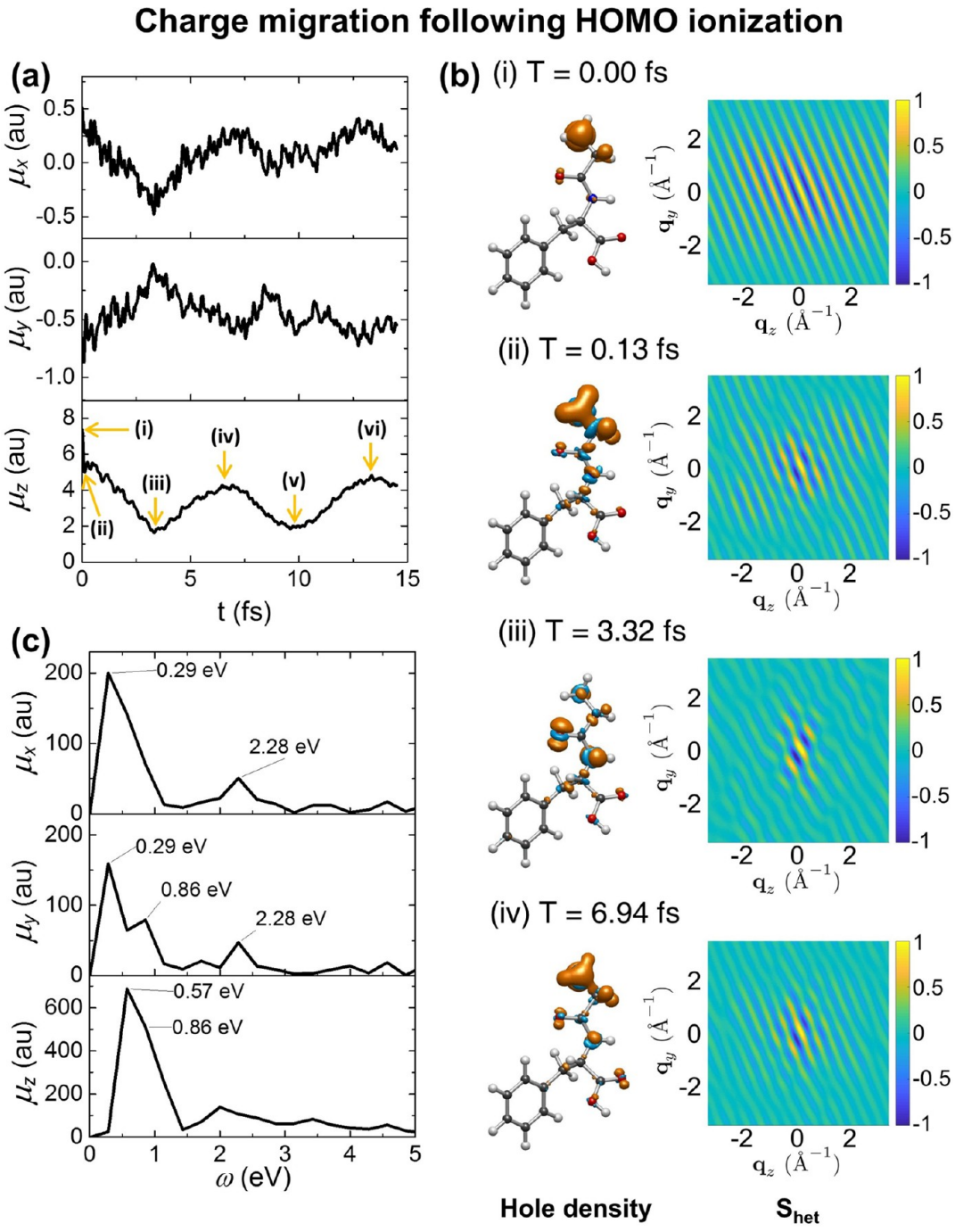

Figure 3. RT-TDDFT simulation of the electron−hole dynamics following HOMO ionization of GF. (a) Time-evolving dipole moments. (b) Snapshots of the hole density (isovalue of 0.006; hole in orange, electron in blue) and the S_{het} signals (eq 4). (c) Fourier transforms of the time-evolving dipole moments.

DOI: 10.1021/acs.jctc.7b00920
J. Chem. Theory Comput. 2018, 14, 329−338

in which $\mathbf{H}^{core}$ is the core Hamiltonian, which is the sum of the nuclear repulsion energy and the one-electron energy; $\mathbf{G}^{J}[\rho(t)]$ is the Coulomb electron repulsion; α, β, and γ are the mixing coefficients for the Hartree−Fock exact exchange $\mathbf{G}^{K}[\rho(t)]$, the DFT exchange $\mathbf{G}^{X\text{-}DFT}[\rho(\mathbf{r},t)]$, and the DFT correlation $\mathbf{G}^{C\text{-}DFT}[\rho(\mathbf{r},t)]$, respectively, for a hybrid DFT functional; and the last term represents the interaction between the system and the ionizing field $\mathbf{E}(t)$ in the dipole approximation, where $\boldsymbol{\mu}$ is the dipole operator.

The expectation value of the charge density $\langle\sigma(\mathbf{r},t)\rangle$ is obtained from the density matrix:

$$\langle\sigma(\mathbf{r},t)\rangle = \sum_{i,j} \psi_i^*(\mathbf{r})\psi_j(\mathbf{r})\rho_{ij}(t) \tag{8}$$

where the ψ_i are the MOs in the neutral ground state. $\langle\sigma(\mathbf{q},t)\rangle$ is then obtained as the spatial Fourier transform of the real-space charge density (see Figure 1). The computational cost for each step in an RT-TDDFT calculation is similar to that for the ground-state self-consistent field calculation for any type of excitation energy range or the ionization of a valence or core electron. This is useful for the study of core-state dynamics in moderate-sized molecules, such as oligopeptides. Equation 6 was integrated using a two-step predictor−corrector scheme:[35,37]

$$\rho(t+\Delta t) = e^{-i\mathbf{F}(t+\Delta t/2)\Delta t}\rho(t)e^{i\mathbf{F}(t+\Delta t/2)\Delta t} \tag{9}$$

The PBE0 exchange−correlation functional[39] and 6-31G(d) basis set were employed in the spin-polarized RT-TDDFT calculations. A time step Δt of 0.2 au (4.84 as) was used for valence ionization. A smaller Δt of 0.02 au (0.484 as) was required for core ionization because of the higher frequencies involved. All of the calculations were performed in the gas phase. The electronic dynamics could be affected by solvent molecules in biologically relevant environments. There are three major solvent effects that could affect the electronic dynamics of the solute: (1) geometrical reorientation of the solvent molecules during the dynamics; (2) random orientations of solvent molecules, generating a unique environment for the solute molecule; and (3) the dielectric environment created by the electron clouds of the solvent molecules. Geometrical reorientation of solvent molecules during the dynamics within 15 fs would be minimal, since it is much slower. The effect of random orientations of solvent molecules on the electronic dynamics of the solute molecule can be taken into account by simulating a number of different configurations and then taking a proper statistical average of them. We plan this for a future study. The effect of the dielectric environment given by the electron clouds of the solvent molecules on the electronic dynamics of the solute molecule can be approximately evaluated by the implicit solvation method, although implicit solvation cannot account for the randomness of the local solvent environment. Conductor-like screening model (COSMO) solvation calculations were performed to investigate the dielectric effect of the water medium on the charge migration of the GF molecule.

The nonstationary ionized state was created by removing an electron from a selected Kohn−Sham orbital i of the neutral molecule without further self-consistent-field procedure, where the electronic and vibrational dynamics are frozen during the ionization process (impulsive ionization):

$$\rho_{ii}^{I} = \rho_{ii}^{N} - 1 \tag{10}$$

where ρ^N and ρ^I are the diagonal density matrices of the neutral molecule and the ion, respectively. The validity of the initial state prepared by an impulsive ionization of a Kohn−Sham orbital was confirmed for core electrons, which are energetically well-separated from the others, with RT-TDDFT calculations.[16] Impulsive ionization of a valence orbital may involve contributions from several orbitals because the energy spacing is smaller than the bandwidth of the ionization pulse. This localized ionization could possibly be achieved by a selective ionization process, as demonstrated by Weinkauf et al.[9] Here we focused on the distinctive features and time scales of electronic dynamics triggered by ionizations in different core and valence orbitals. The ionization pulse was not treated explicitly. More rigorously, ionization is a many-electron process. The ionized state can be expressed as a superposition of ionized states with coefficients based on the ionization amplitude, which depends on the pump field envelope.[10] The probe pulse envelopes $\mathcal{A}_d$, $\mathcal{A}_1$, and $\mathcal{A}_2$ were approximated by delta functions.

3. CHARGE MIGRATION IN GLYCINE−PHENYLALANINE FOLLOWING VALENCE IONIZATION

The GF dipeptide has a benzene chromophore in the Phe side and a short saturated carbon bridge in the Gly side. A nitrogen lone pair of electrons on the N-terminal amine is located in the Gly side. The molecular orbitals (MOs) of the N lone pair and the benzene chromophore constitute the highest occupied MO (HOMO) and HOMO−1, respectively (Figure 2), with an energy spacing of 0.21 eV. Since the two orbitals are spatially well-separated, site-specific valence ionization can be detected by X-ray diffraction. The electron-donating group, an amide and a carboxylate, can participate in the charge migration dynamics. We study how the existence of the electron-rich group affects the charge (hole) migration dynamics. The hole density created by ionizing one of the two valence orbitals will oscillate back and forth between the initial location and electron-donating groups along the dipeptide backbone, which is aligned along the z axis. Because of the nonbonding character of these valence MOs, the effect of nuclear motion on the early dynamics is weak. The 15 fs charge migration dynamics triggered by the ionization of either of the two valence electrons was simulated.

Figure 3 shows the simulation after an electron is removed from the HOMO, which is mostly localized on the N-terminal NH_2. The dipole moment along the z axis, μ_z, shows temporal oscillation. Charge migration along z (see Figure 2 for definition of the coordinates), as indicated by μ_z, dominates the x and y components with a strong oscillation, as shown in Figure 3a. This oscillation starts after an initial 130 as decay. A similar time scale was observed for the ultrafast initial decay after HOMO−1 ionization and the core ionizations. Key points are

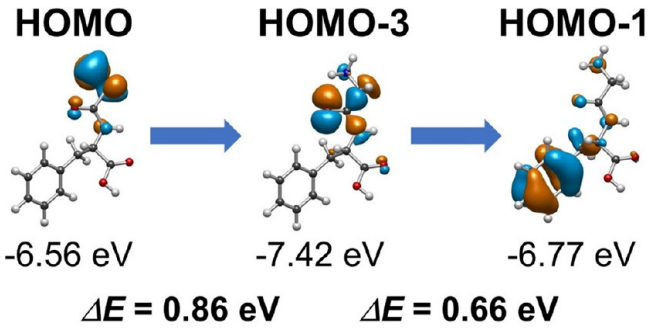

Figure 4. Pairs of molecular orbitals responsible for the beating pattern after HOMO ionization of GF. Isovalue of 0.04. Arrows indicate the flow of the charge migration.

DOI: 10.1021/acs.jctc.7b00920
J. Chem. Theory Comput. 2018, 14, 329−338

marked as i−vi in Figure 3. The ultrafast dynamics occurs along i−ii and the subsequent charge oscillation along ii−iv. The charge oscillation along the dynamics i−iv is displayed in Figure 3b. In i−ii, a small amount of hole density spreads over the hydrogen atoms in the N-terminal NH_2 moiety and the GF backbone, while the majority of the hole density stays at the initial NH_2 site. The hole density then migrates from NH_2 to the oxygen and nitrogen atoms of the amide bond. The electron has thus migrated from the electron-rich amide to the electron-deficient NH_2 group at T = 3.32 fs. This migration takes 3.19 fs, and the hole density at NH_2 is significantly decreased. The hole then migrates back to the NH_2 (iii−iv) by T = 6.94 fs, leaving a small hole density at the carboxyl group (−COOH) so that the electronic structures of ii and iv are not exactly the same. However, the hole density does not spread into the phenyl group because of the potential barrier. This feature is marked by the damped decay of the time-evolving dipole moment μ_z (Figure 3a). The charge oscillates back and forth with a period of 6.81 fs, which is slightly longer than that in phenylalanine monomer (4.5 fs)[10] because of the elongated glycine bridge. As shown in Figure S9 in the Supporting Information, COSMO solvation of the dipeptide in water does not significantly change the charge migration dynamics.

The heterodyne X-ray diffraction signal (S_{het}) can detect the charge oscillation along the ionization dynamics (see Figures S1 and S2 for the S_{hom} and S_{het} signals for the hole and the total electron density). The initially localized hole density at the amine site generates a strong diffraction signal (i), which

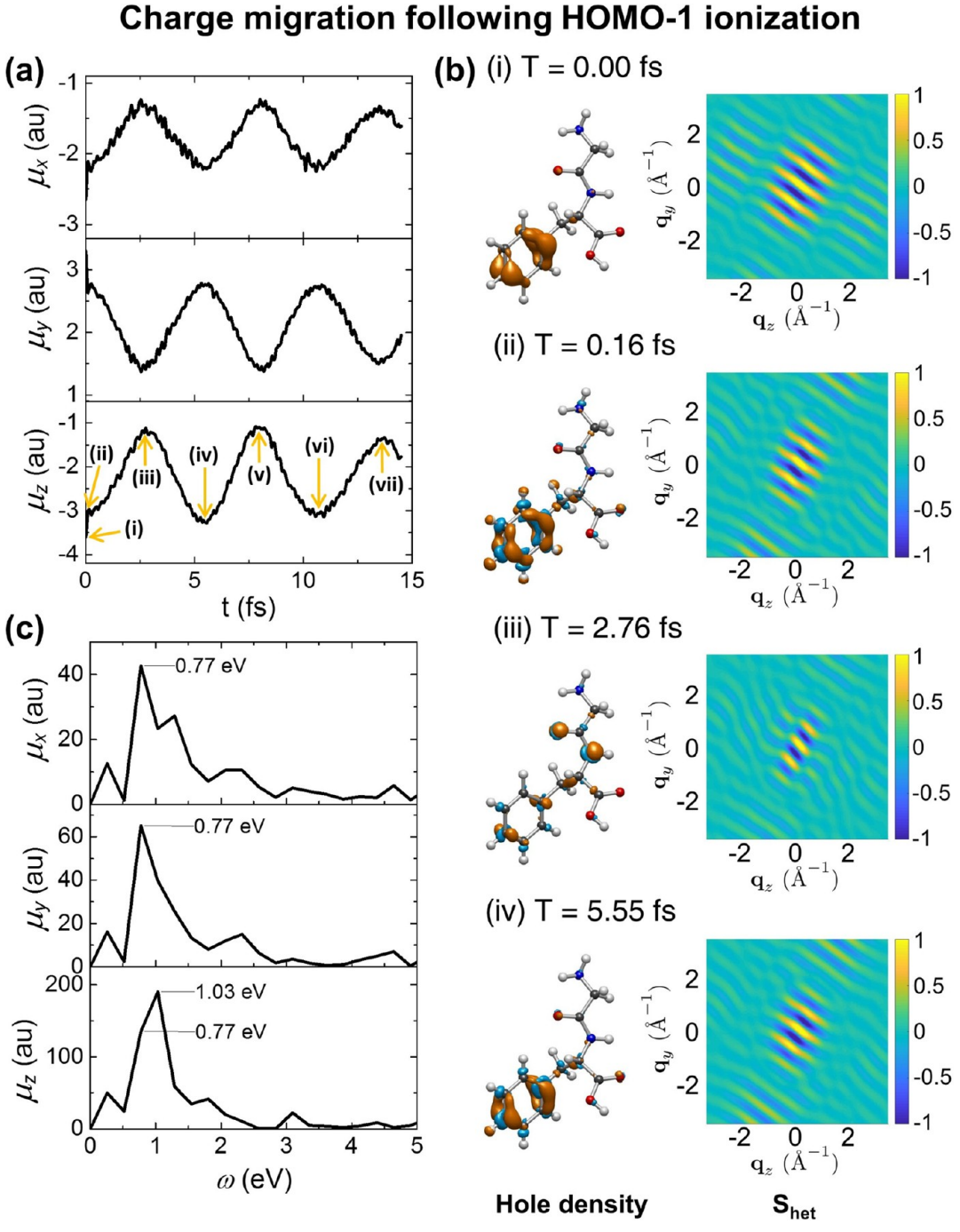

Figure 5. Same as Figure 3 but for the HOMO−1 ionization.

DOI: 10.1021/acs.jctc.7b00920
J. Chem. Theory Comput. 2018, 14, 329−338

becomes weaker as the hole density spreads along the GF chain during the ultrafast initial decay (ii). The signal further decreases upon the migration of the major hole density from the amine site to the amide site. Spreading the hole density in real space causes reduction of the diffraction signal in **q** space. The dynamical features of the charge migration can be monitored by the S_{het} signal. The most significant feature is the change in the diffraction pattern in the q_x/q_y plane, since the charge migration occurs along the z axis in real space.

The temporal Fourier transforms of the time-evolving dipole moments μ_x, μ_y, and μ_z after HOMO ionization (shown in Figure 3c) carry detailed information regarding the charge migration. The most significant contribution to μ_z is the beating between 0.57 and 0.86 eV; the hole oscillates between HOMO−1 and HOMO−3 with ΔE = 0.66 eV (6.3 fs) and between the HOMO and HOMO−3 with ΔE = 0.86 eV (4.8 fs) (see Figure 4). This indicates that the hole initially created at the HOMO propagates through the dipeptide backbone via HOMO−3 to HOMO−1. Electron correlation between the initial hole at the N lone-pair orbital at the terminal amine site (HOMO) and the delocalized C═O antibonding orbital (HOMO−3) allows the charge migration across the dipeptide. The time scale and the spatial features of the total hole migrations along i−iv are well-understood in terms of the mixture of the hole migrations between the two pairs. We conclude that HOMO ionization creates charge oscillation among the low-lying valence orbitals down to 5 eV below the HOMO.

Figure 5 shows a similar simulation but for an impulsive ionization of HOMO−1, which is mostly localized on the phenyl ring. Ultrafast decay takes place by T = 0.16 fs, where a small amount of hole density spreads over the benzyl hydrogen atoms and the GF chain and significant electron density grows at the benzyl carbons. Again, we note an ultrafast 160 as redistribution of electron−hole density in a local area. Most of the hole density then migrates from the phenyl group to the amide (particularly oxygen and nitrogen) by T = 2.76 fs. A feature similar to that in the HOMO ionization was found at T = 5.55 fs: the charge migrates back to the phenyl group, where the initial hole density was created. It then oscillates back and forth with a period of 5.39 fs. The charge oscillations after the HOMO (6.81 fs) and HOMO−1 (5.39 fs) ionizations occur on a similar time scale. The Fourier transform of the beating pattern in the time-evolving dipole moments is shown in Figure 5c, and the corresponding pairs of MOs are displayed in Figure 6.

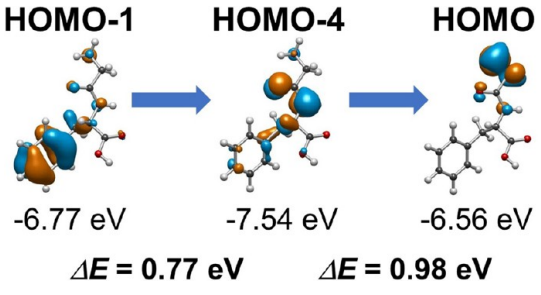

Figure 6. Pairs of molecular orbitals responsible for the beating pattern after HOMO−1 ionization of GF. Isovalue of 0.04. Arrows indicate the flow of the charge migration.

The heterodyne X-ray diffraction signal (S_{het}) reproduces the features of the charge oscillation in the ion (see Figures S3 and S4 for the S_{hom} and S_{het} signals for the hole and the total electron density). The initially localized hole density at the phenyl site generates a strong diffraction signal (i). The diffraction pattern is distinct from that of the HOMO ionization located at the N-terminal amine site. The signal is further reduced as the hole density spreads along the GF chain in the ultrafast initial decay (i). It then decays as the major hole density migrates from the phenyl site to the amide site (ii−iii) and reaches its minimum. Then the signal grows following the hole migration back to the phenyl site (iii−iv).

The Fourier transforms of the time-evolving dipole moments following HOMO−1 ionization are shown in Figure 5c, and the corresponding pairs of MOs are displayed in Figure 6. Charge oscillations between 0.77 to 1.03 eV play a major role in the total charge migration dynamics; the hole oscillates between HOMO−4 and HOMO−1 with ΔE = 0.77 eV (5.3 fs) and between HOMO−4 and the HOMO with ΔE = 0.98 eV (4.2 fs). This indicates that the hole initially created at benzene chromophore (HOMO−1) propagates through the dipeptide chain mediated by the lone-pair electrons at oxygen and nitrogen of the peptide bond (HOMO−4) delocalized to benzene and the N lone-pair at the N-terminal amine (HOMO). Overall, the charge migration following the ionization of the benzene chromophore (HOMO−1) is faster compared with that following the ionization of the N lone pair at the N-terminal amine (HOMO), reflecting the higher energy difference of the relevant orbitals.

4. ELECTRON DYNAMICS IN GLYCINE−PHENYLALANINE FOLLOWING CORE IONIZATION

In this section, we present the charge migration dynamics in GF following ionization of an amide O 1s or N-terminal amine N 1s electron (Figure 7). Core ionization dynamics is element- and

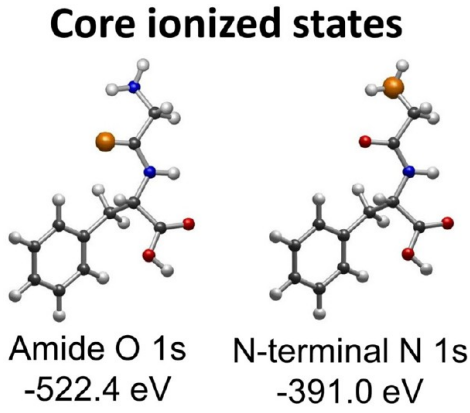

Figure 7. Core amide O 1s and N-terminal N 1s molecular orbitals (isovalue of 0.04).

site-specific thanks to the highly localized nature of the core orbitals. A core hole induces a much more pronounced charge migration between many electronic states and on a much faster time scale. We have limited the charge migration dynamics following the ionization of either of the two core states up to 3.6 fs to safely exclude nuclear motions.

Figure 8 presents the charge migration following the impulsive ionization of the amide oxygen K edge. The time-evolving dipole moment μ_z (Figure 8a) shows a fast decay with a complex oscillating pattern, indicating the participation of many MO pairs. An ultrafast initial decay (0.11 fs) is followed by a blurred charge oscillation along the z axis. The decays of μ_x, μ_y, and μ_z are distinct and out-of-phase from each other, indicating contributions from many electronic transitions with

DOI: 10.1021/acs.jctc.7b00920
J. Chem. Theory Comput. 2018, 14, 329−338

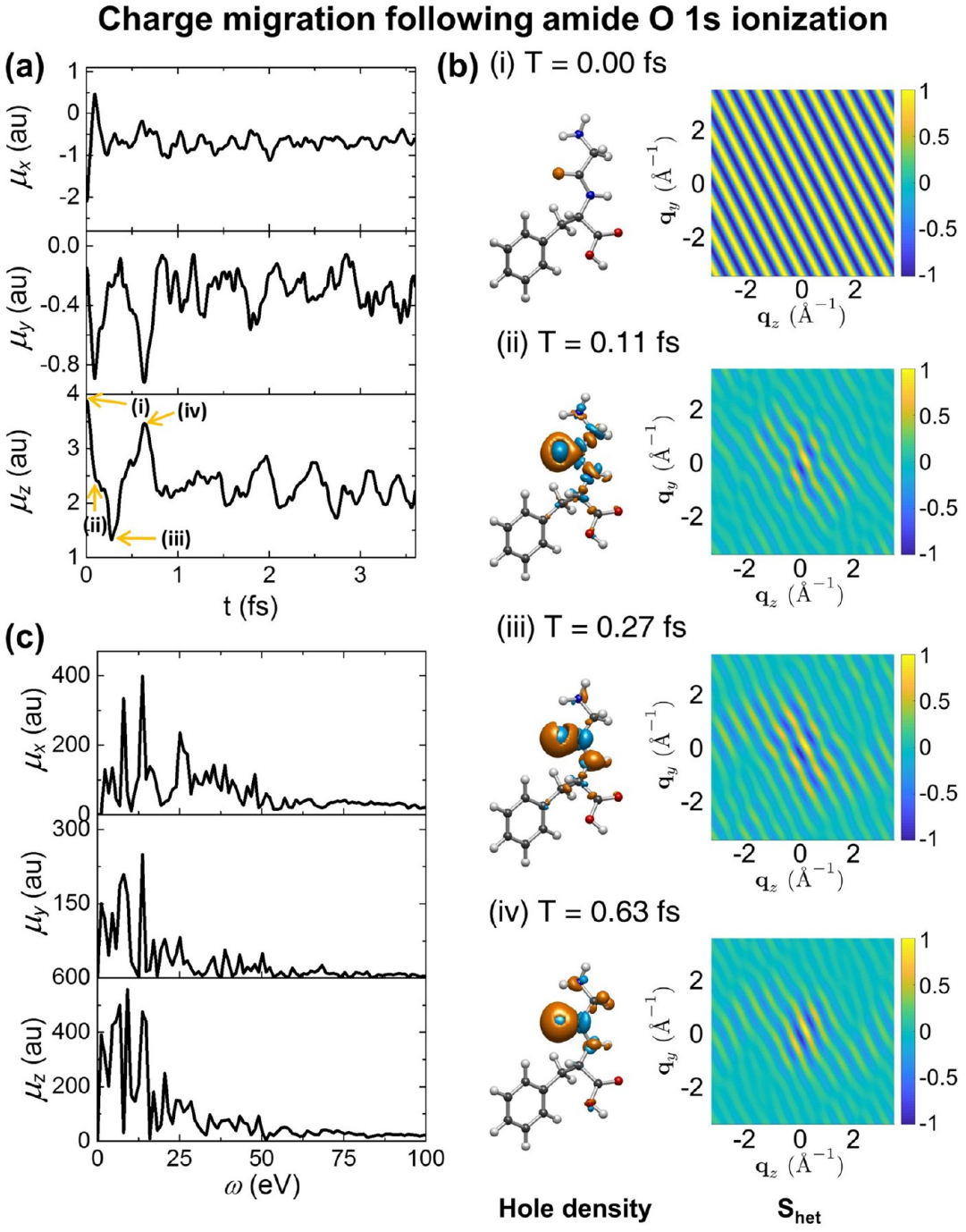

Figure 8. Same as Figure 3 but for the amide O 1s ionization. Isovalue of 0.01 for the hole density.

different frequencies. Figure 8b shows the time-evolving hole density and S_{het} signals. The initial hole density localized at the amide O site quickly spreads in space, showing a more pronounced charge migration than the valence ionizations (note the isovalue of 0.01 in Figures 8 and 9 vs 0.006 in Figures 3 and 5). Most of the hole density, however, remains at the initial site and the nearby amide, while many valence states participate in the charge migration. A similar feature in the charge migration was calculated for the N 1s core ionization in nitrosobenzene.[16,40] The complexity arises from the fact that the core ionization triggers many decay processes throughout the valence to core electron regime. This is supported by the Fourier transforms of the time-evolving dipole moments (Figure 8c), which reveal contributions from electronic transitions with higher energy (up to 100 eV). In the inner- and outer-valence regimes, strong signatures of charge oscillation in various MO pairs are observed.

The S_{het} signal shows an elongated pattern in reciprocal space due to the localized nature of the core ionization in real space (see Figures S5 and S6 for the S_{hom} and S_{het} signals for the hole and the total electron density). The elongated signal quickly decays upon ultrafast initial decay, and then the signal elongates and diminishes repeatedly.

Figure 9 displays the results for the impulsive ionization of the N-terminal N 1s orbital. The dipole moments show a complex evolution pattern with significant oscillation (Figure 9a), similar to the amide O 1s core ionization. An ultrafast 0.11 fs initial decay precedes the complex time evolution of the core-ionized system. The initial hole density spreads along the GF chain in 0.11 fs (i),

DOI: 10.1021/acs.jctc.7b00920
J. Chem. Theory Comput. 2018, 14, 329−338

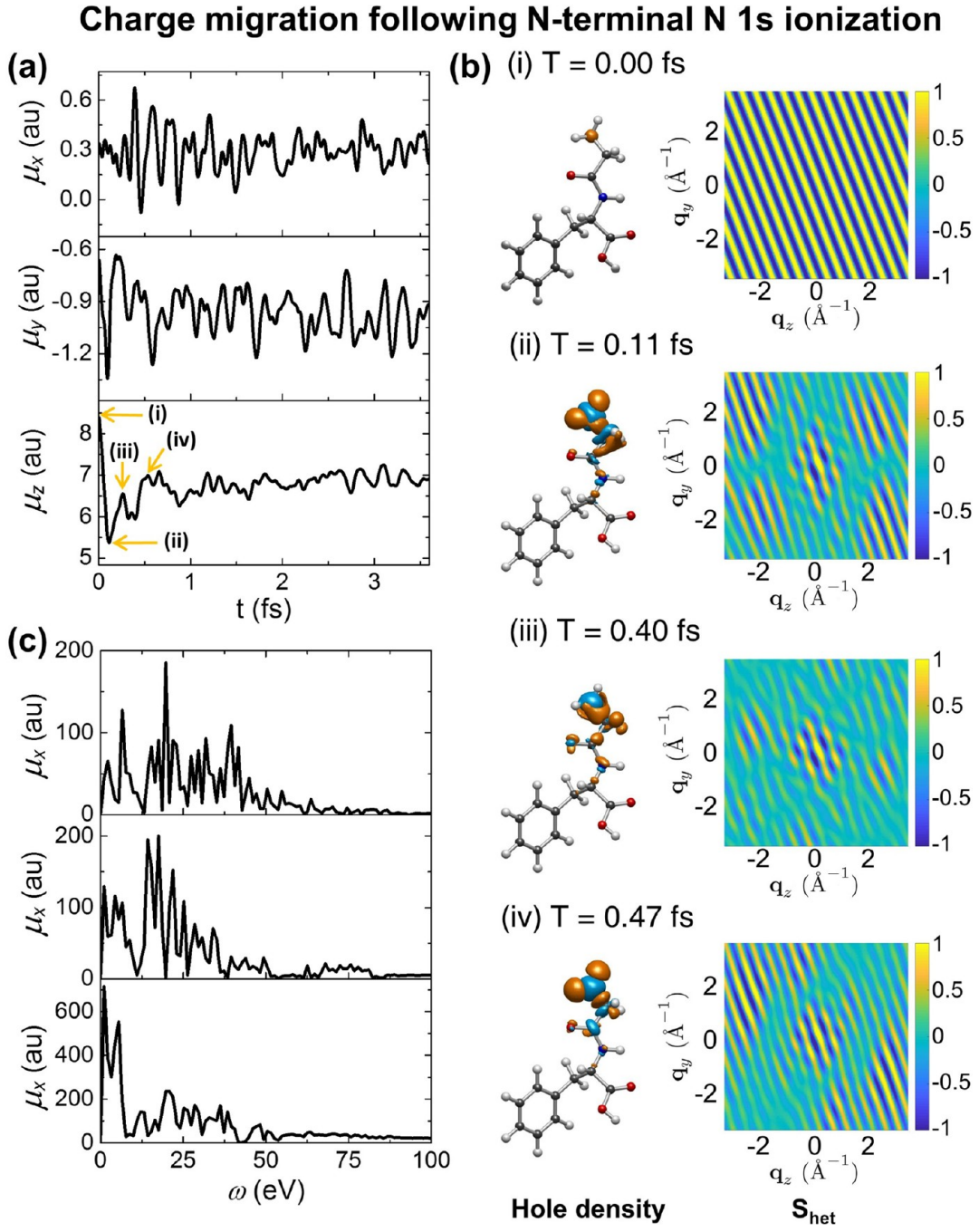

Figure 9. Same as Figure 3 but for the N-terminal N 1s ionization. Isovalue of 0.01 for the hole density.

and the following change occurred mostly on the NH_2 (Figure 9b). Again, most of the hole density created in the initial ultrafast dynamics remains localized at the amine, while valence states induce a dramatic change in the electronic charge density. Sub-500 as charge oscillation is observed. The temporal Fourier transforms of the dipole moments reveal that many high-energy electronic transitions (up to 100 eV) participate the decay of the system (Figure 9c). The S_{het} signals show complicated time-evolving features following the N 1s ionization (see Figures S7 and S8 for the S_{hom} and S_{het} signals for the hole and the total electron density).

5. CONCLUSIONS

We have simulated the time-resolved X-ray diffraction signals from impulsively created ions using RT-TDDFT. In a previous study,[41] we had calculated such signals in glycine by expanding it in eigenstates of the ionic states. This required calculation of all of the matrix elements between the various excited states, which is computationally expensive and becomes intractable for large molecules. The RT-TDDFT approach, in contrast, avoids the tedious calculation of core and valence excited states in modeling the charge density dynamics. Direct solution of equations of motion for the reduced single-electron density matrix $\rho(t)$ provides a convenient way to simulate the electronic dynamics. Heterodyne-detected X-ray diffraction signals allow for real-space, real-time determination of time-evolving difference densities such as the hole density.

We have simulated the ultrafast charge migration dynamics following impulsive ionization of the GF dipeptide over a broad

DOI: 10.1021/acs.jctc.7b00920
J. Chem. Theory Comput. 2018, 14, 329−338

range of electronic energies. Pure electronic dynamics has been simulated following the ionization of valence or core electrons. The simulations provide clear pictures of the charge migration in the dipeptide with a sub-7 fs time scale for valence ionization and sub-500 as time scale for core ionization. Site-specific valence (N nonbonding and phenyl chromophore) ionizations localized at each end of the dipeptide induce charge migration from the initially created hole site to the electron-donating amide group. Core ionization of either the amide O 1s or amine N 1s electrons induces significant charge migration among the valence states, while the majority of the hole density stays at the initial site.

The simulation yields observables such as the time-evolving dipole moment, time-evolving charge density $\langle\sigma(\mathbf{r},t)\rangle$, and time-resolved X-ray diffraction signals that can be measured by existing X-ray technology. Adding nuclear Ehrenfest dynamics would be a future extension of this work. Also, inclusion of the optical and X-ray fields in the equations of motion makes it to calculate specific nonlinear optical signals selected by a phase-cycling algorithm.[42]

■ ASSOCIATED CONTENT

Supporting Information

The Supporting Information is available free of charge on the ACS Publications website at DOI: 10.1021/acs.jctc.7b00920.

S_{hom} and S_{het} signals for the hole and the total density following valence and core ionizations and the effect of COSMO solvation on the dipole moments following valence and core ionizations (PDF)

■ AUTHOR INFORMATION

Corresponding Authors

*E-mail: daeheumc@uci.edu.
*E-mail: jinylee@skku.edu.
*E-mail: smukamel@uci.edu.

ORCID

Daeheum Cho: 0000-0002-0322-4291
Jin Yong Lee: 0000-0003-0360-5059
Shaul Mukamel: 0000-0002-6015-3135

Funding

Support by the Chemical Sciences, Geosciences, and Biosciences Division, Office of Basic Energy Sciences, Office of Science, U.S. Deparment of Energy (Award DE-FG02-04ER15571) and by the National Science Foundation (Grant CHE-1663822) is gratefully acknowledged. J.R.R. was supported by the DOE grant.

Notes

The authors declare no competing financial interest.

■ REFERENCES

(1) Schotte, F.; Lim, M.; Jackson, T. A.; Smirnov, A. V.; Soman, J.; Olson, J. S.; Phillips, G. N., Jr.; Wulff, M.; Anfinrud, P. A. Watching a Protein as it Functions with 150-ps Time-Resolved X-ray Crystallography. *Science* **2003**, *300*, 1944−1947.

(2) Chapman, H. N.; Fromme, P.; Barty, A.; White, T. A.; Kirian, R. A.; Aquila, A.; Hunter, M. S.; Schulz, J.; DePonte, D. P.; Weierstall, U.; Doak, R. B.; Maia, F. R. N. C.; Martin, A. V.; Schlichting, I.; Lomb, L.; Coppola, N.; Shoeman, R. L.; Epp, S. W.; Hartmann, R.; Rolles, D.; Rudenko, A.; Foucar, L.; Kimmel, N.; Weidenspointner, G.; Holl, P.; Liang, M.; Barthelmess, M.; Caleman, C.; Boutet, S.; Bogan, M. J.; Krzywinski, J.; Bostedt, C.; Bajt, S.; Gumprecht, L.; Rudek, B.; Erk, B.; Schmidt, C.; Homke, A.; Reich, C.; Pietschner, D.; Struder, L.; Hauser, G.; Gorke, H.; Ullrich, J.; Herrmann, S.; Schaller, G.; Schopper, F.; Soltau, H.; Kuhnel, K.-U.; Messerschmidt, M.; Bozek, J. D.; Hau-Riege, S. P.; Frank, M.; Hampton, C. Y.; Sierra, R. G.; Starodub, D.; Williams, G. J.; Hajdu, J.; Timneanu, N.; Seibert, M. M.; Andreasson, J.; Rocker, A.; Jonsson, O.; Svenda, M.; Stern, S.; Nass, K.; Andritschke, R.; Schroter, C.-D.; Krasniqi, F.; Bott, M.; Schmidt, K. E.; Wang, X.; Grotjohann, I.; Holton, J. M.; Barends, T. R. M.; Neutze, R.; Marchesini, S.; Fromme, R.; Schorb, S.; Rupp, D.; Adolph, M.; Gorkhover, T.; Andersson, I.; Hirsemann, H.; Potdevin, G.; Graafsma, H.; Nilsson, B.; Spence, J. C. H. Femtosecond X-ray protein nanocrystallography. *Nature* **2011**, *470*, 73−77.

(3) Seibert, M. M.; Ekeberg, T.; Maia, F. R. N. C.; Svenda, M.; Andreasson, J.; Jonsson, O.; Odic, D.; Iwan, B.; Rocker, A.; Westphal, D.; Hantke, M.; DePonte, D. P.; Barty, A.; Schulz, J.; Gumprecht, L.; Coppola, N.; Aquila, A.; Liang, M.; White, T. A.; Martin, A.; Caleman, C.; Stern, S.; Abergel, C.; Seltzer, V.; Claverie, J.-M.; Bostedt, C.; Bozek, J. D.; Boutet, S.; Miahnahri, A. A.; Messerschmidt, M.; Krzywinski, J.; Williams, G.; Hodgson, K. O.; Bogan, M. J.; Hampton, C. Y.; Sierra, R. G.; Starodub, D.; Andersson, I.; Bajt, S.; Barthelmess, M.; Spence, J. C. H.; Fromme, P.; Weierstall, U.; Kirian, R.; Hunter, M.; Doak, R. B.; Marchesini, S.; Hau-Riege, S. P.; Frank, M.; Shoeman, R. L.; Lomb, L.; Epp, S. W.; Hartmann, R.; Rolles, D.; Rudenko, A.; Schmidt, C.; Foucar, L.; Kimmel, N.; Holl, P.; Rudek, B.; Erk, B.; Homke, A.; Reich, C.; Pietschner, D.; Weidenspointner, G.; Struder, L.; Hauser, G.; Gorke, H.; Ullrich, J.; Schlichting, I.; Herrmann, S.; Schaller, G.; Schopper, F.; Soltau, H.; Kuhnel, K.-U.; Andritschke, R.; Schroter, C.-D.; Krasniqi, F.; Bott, M.; Schorb, S.; Rupp, D.; Adolph, M.; Gorkhover, T.; Hirsemann, H.; Potdevin, G.; Graafsma, H.; Nilsson, B.; Chapman, H. N.; Hajdu, J. Single mimivirus particles intercepted and imaged with an X-ray laser. *Nature* **2011**, *470*, 78−81.

(4) Ihee, H.; Lorenc, M.; Kim, T. K.; Kong, Q. Y.; Cammarata, M.; Lee, J. H.; Bratos, S.; Wulff, M. Ultrafast X-ray Diffraction of Transient Molecular Structures in Solution. *Science* **2005**, *309*, 1223−1227.

(5) Baczewski, A. D.; Shulenburger, L.; Desjarlais, M. P.; Hansen, S. B.; Magyar, R. J. X-ray Thomson Scattering in Warm Dense Matter without the Chihara Decomposition. *Phys. Rev. Lett.* **2016**, *116*, 115004.

(6) Siders, C. W.; Cavalleri, A.; Sokolowski-Tinten, K.; Tóth, C.; Guo, T.; Kammler, M.; Horn von Hoegen, M.; Wilson, K. R.; von der Linde, D.; Barty, C. P. J. Detection of Nonthermal Melting by Ultrafast X-ray Diffraction. *Science* **1999**, *286*, 1340−1342.

(7) Cammarata, M.; Levantino, M.; Schotte, F.; Anfinrud, P. A.; Ewald, F.; Choi, J.; Cupane, A.; Wulff, M.; Ihee, H. Tracking the structural dynamics of proteins in solution using time-resolved wide-angle X-ray scattering. *Nat. Methods* **2008**, *5*, 881−886.

(8) Kowalewski, M.; Bennett, K.; Mukamel, S. Monitoring non-adiabatic avoided crossing dynamics in molecules by ultrafast X-ray diffraction. *Struct. Dyn.* **2017**, *4*, 054101.

(9) Weinkauf, R.; Schanen, P.; Yang, D.; Soukara, S.; Schlag, E. W. Elementary Processes in Peptides: Electron Mobility and Dissociation in Peptide Cations in the Gas Phase. *J. Phys. Chem.* **1995**, *99*, 11255−11265.

(10) Calegari, F.; Ayuso, D.; Trabattoni, A.; Belshaw, L.; De Camillis, S.; Anumula, S.; Frassetto, F.; Poletto, L.; Palacios, A.; Decleva, P.; Greenwood, J. B.; Martín, F.; Nisoli, M. Ultrafast electron dynamics in phenylalanine initiated by attosecond pulses. *Science* **2014**, *346*, 336−339.

(11) Belshaw, L.; Calegari, F.; Duffy, M. J.; Trabattoni, A.; Poletto, L.; Nisoli, M.; Greenwood, J. B. Observation of Ultrafast Charge Migration in an Amino Acid. *J. Phys. Chem. Lett.* **2012**, *3*, 3751−3754.

(12) Cederbaum, L.; Zobeley, J. Ultrafast charge migration by electron correlation. *Chem. Phys. Lett.* **1999**, *307*, 205−210.

(13) Lünnemann, S.; Kuleff, A. I.; Cederbaum, L. S. Ultrafast electron dynamics following outer-valence ionization: The impact of low-lying relaxation satellite states. *J. Chem. Phys.* **2009**, *130*, 154305.

(14) Remacle, F.; Levine, R. D. An electronic time scale in chemistry. *Proc. Natl. Acad. Sci. U. S. A.* **2006**, *103*, 6793−6798.

(15) López-Tarifa, P.; Hervé du Penhoat, M.-A.; Vuilleumier, R.; Gaigeot, M.-P.; Rothlisberger, U.; Tavernelli, I.; Le Padellec, A.; Champeaux, J.-P.; Alcamí, M.; Moretto-Capelle, P.; Martín, F.; Politis,

DOI: 10.1021/acs.jctc.7b00920
J. Chem. Theory Comput. 2018, 14, 329−338

M.-F. Time-dependent density functional theory molecular dynamics simulation of doubly charged uracil in gas phase. *Cent. Eur. J. Phys.* **2014**, *12*, 97−102.
(16) Bruner, A.; Hernandez, S.; Mauger, F.; Abanador, P. M.; LaMaster, D. J.; Gaarde, M. B.; Schafer, K. J.; Lopata, K. Attosecond Charge Migration with TDDFT: Accurate Dynamics from a Well-Defined Initial State. *J. Phys. Chem. Lett.* **2017**, *8*, 3991−3996.
(17) Bennett, K.; Biggs, J. D.; Zhang, Y.; Dorfman, K. E.; Mukamel, S. Time-, frequency-, and wavevector-resolved x-ray diffraction from single molecules. *J. Chem. Phys.* **2014**, *140*, 204311.
(18) Kulander, K. C. Time-dependent Hartree-Fock theory of multiphoton ionization: Helium. *Phys. Rev. A: At., Mol., Opt. Phys.* **1987**, *36*, 2726−2738.
(19) Runge, E.; Gross, E. K. U. Density-Functional Theory for Time-Dependent Systems. *Phys. Rev. Lett.* **1984**, *52*, 997−1000.
(20) Nascimento, D. R.; DePrince, A. E. Simulation of Near-Edge X-ray Absorption Fine Structure with Time-Dependent Equation-of-Motion Coupled-Cluster Theory. *J. Phys. Chem. Lett.* **2017**, *8*, 2951−2957.
(21) Meyer, H.-D.; Manthe, U.; Cederbaum, L. S. The multi-configurational time-dependent Hartree approach. *Chem. Phys. Lett.* **1990**, *165*, 73−78.
(22) Helgaker, T.; Uggerud, E.; Jensen, H. J. A. Integration of the classical equations of motion on ab initio molecular potential energy surfaces using gradients and Hessians: application to translational energy release upon fragmentation. *Chem. Phys. Lett.* **1990**, *173*, 145−150.
(23) Herman, M. F. Nonadiabatic semiclassical scattering. I. Analysis of generalized surface hopping procedures. *J. Chem. Phys.* **1984**, *81*, 754−763.
(24) Tully, J. C. Molecular dynamics with electronic transitions. *J. Chem. Phys.* **1990**, *93*, 1061−1071.
(25) Yabana, K.; Bertsch, G. F. Time-dependent local-density approximation in real time. *Phys. Rev. B: Condens. Matter Mater. Phys.* **1996**, *54*, 4484−4487.
(26) Kosloff, R. Time-dependent quantum-mechanical methods for molecular dynamics. *J. Phys. Chem.* **1988**, *92*, 2087−2100.
(27) Castro, A.; Marques, M. A. L.; Rubio, A. Propagators for the time-dependent Kohn-Sham equations. *J. Chem. Phys.* **2004**, *121*, 3425−3433.
(28) Zhang, Y.; Hua, W.; Bennett, K.; Mukamel, S. *Top. Curr. Chem.* **2014**, *368*, 273−345.
(29) Tussupbayev, S.; Govind, N.; Lopata, K.; Cramer, C. J. Comparison of Real-Time and Linear-Response Time-Dependent Density Functional Theories for Molecular Chromophores Ranging from Sparse to High Densities of States. *J. Chem. Theory Comput.* **2015**, *11*, 1102−1109.
(30) Akama, T.; Imamura, Y.; Nakai, H. Application of Real-time Time-dependent Density Functional Theory with the CVB3LYP Functional to Core Excitations. *Chem. Lett.* **2010**, *39*, 407−409.
(31) Donati, G.; Lingerfelt, D. B.; Petrone, A.; Rega, N.; Li, X. Watching Polaron Pair Formation from First-Principles Electron-Nuclear Dynamics. *J. Phys. Chem. A* **2016**, *120*, 7255−7261.
(32) Petrone, A.; Lingerfelt, D. B.; Rega, N.; Li, X. From charge-transfer to a charge-separated state: a perspective from the real-time TDDFT excitonic dynamics. *Phys. Chem. Chem. Phys.* **2014**, *16*, 24457−24465.
(33) Peng, B.; Lingerfelt, D. B.; Ding, F.; Aikens, C. M.; Li, X. Real-Time TDDFT Studies of Exciton Decay and Transfer in Silver Nanowire Arrays. *J. Phys. Chem. C* **2015**, *119*, 6421−6427.
(34) Govind, N.; Lopata, K.; Rousseau, R.; Andersen, A.; Kowalski, K. Visible Light Absorption of N-Doped TiO2 Rutile Using (LR/RT)-TDDFT and Active Space EOMCCSD Calculations. *J. Phys. Chem. Lett.* **2011**, *2*, 2696−2701.
(35) Cheng, C.-L.; Evans, J. S.; Van Voorhis, T. Simulating molecular conductance using real-time density functional theory. *Phys. Rev. B: Condens. Matter Mater. Phys.* **2006**, *74*, 155112.
(36) Valiev, M.; Bylaska, E. J.; Govind, N.; Kowalski, K.; Straatsma, T. P.; Van Dam, H. J. J.; Wang, D.; Nieplocha, J.; Apra, E.; Windus, T. L.; de Jong, W. A. NWChem: A comprehensive and scalable open-source solution for large scale molecular simulations. *Comput. Phys. Commun.* **2010**, *181*, 1477−1489.
(37) Lopata, K.; Govind, N. Modeling Fast Electron Dynamics with Real-Time Time-Dependent Density Functional Theory: Application to Small Molecules and Chromophores. *J. Chem. Theory Comput.* **2011**, *7*, 1344−1355.
(38) Tretiak, S.; Mukamel, S. Density Matrix Analysis and Simulation of Electronic Excitations in Conjugated and Aggregated Molecules. *Chem. Rev.* **2002**, *102*, 3171−3212.
(39) Perdew, J. P.; Burke, K.; Ernzerhof, M. Generalized Gradient Approximation Made Simple. *Phys. Rev. Lett.* **1996**, *77*, 3865−3868.
(40) Kuleff, A. I.; Kryzhevoi, N. V.; Pernpointner, M.; Cederbaum, L. S. Core Ionization Initiates Subfemtosecond Charge Migration in the Valence Shell of Molecules. *Phys. Rev. Lett.* **2016**, *117*, 093002.
(41) Zhang, Y.; Biggs, J. D.; Hua, W.; Dorfman, K. E.; Mukamel, S. Three-dimensional attosecond resonant stimulated X-ray Raman spectroscopy of electronic excitations in core-ionized glycine. *Phys. Chem. Chem. Phys.* **2014**, *16*, 24323−24331.
(42) Hamm, P.; Zanni, M. *Concepts and Methods of 2D Infrared Spectroscopy*; Cambridge University Press: Cambridge, U.K., 2011.

DOI: 10.1021/acs.jctc.7b00920
J. Chem. Theory Comput. 2018, 14, 329−338